MEDDOCS Open Access Publisher

ISSN: 2578-8760

Journal of Nanomedicine

Open Access | Research Article

Bioactive Nano Hydroxyapatites for Orbital Floor Repair and Regeneration

*FH Alhamoudi[1,3]; H Akhtar[4]; Y Almoshawah[2,3]; AC Talari[3]; AA Chaudhry[5]; GC Reilly[4]; I U Rehman[3]**

[1]Dental Technology Department, King Khalid University, KSA.

[2]Mechanical Engineering Department, Shaqra University, KSA.

[3]Engineering Department, Lancaster University, UK.

[4]INSIGNEO institute for in silico Medicine, University of Sheffield, UK.

[5]Interdisciplinary Research Centre in Biomedical Materials (IRCBM), Pakistan.

Corresponding Author(s): Ihtesham ur Rehman

Engineering Department, Faculty of Science and Technology, Lancaster University, Gillow Avenue, Lancaster, LA1 4YW, UK.

Tel: +44-0-1524-594038;

Email: i.u.rehman@lancaster.ac.uk

Received: Apr 01, 2021

Accepted: May 14, 2021

Published Online: May 17, 2021

Journal: Journal of Nanomedicine

Publisher: MedDocs Publishers LLC

Online edition: http://meddocsonline.org/

Keywords: Hydroxyapatite; Nano-bioceramics; Synthesis; Ionic substitution; Chemical; Physical and biological characterisation.

Abstract

Bioactive nano-hydroxyapatites have been synthesised for orbital floor repair and regeneration. Hydroxyapatite (HA) is widely used for bone repair and regeneration. It is composed of multiple anionic and cationic species, such as carbonate, fluoride, phosphate, sodium, magnesium, silicon and citrate. However, the development of bioactive materials that can repair and regenerate bone is crucial for orbital floor fracture repair. Different ionic-substituted hydroxyapatites that included carbonate, fluoride and citrate were prepared by using a low-temperature hydrothermal flow process and their chemical and physical properties evaluated. Biological properties were evaluated by analysing cell viability of these synthesised materials by Alamar Blue cell metabolic activity assay with two different cell lines (MG63 and HTERT-BMSC's). Results confirmed that ionic substitution with fluoride and citrate improved biocompatibility and cell viability of synthesised hydroxyapatites.

Introduction

Bone repair and regeneration is required as consequence of bone losses due to trauma or disease. It has been reported that fractures in orbital regions and facial bone are the most common midfacial fractures [1-3], where orbital floor fracture is the most common fracture (accounting for 50.2%) among the orbital's walls (roof, lateral and medial) [3] (Figure 1).

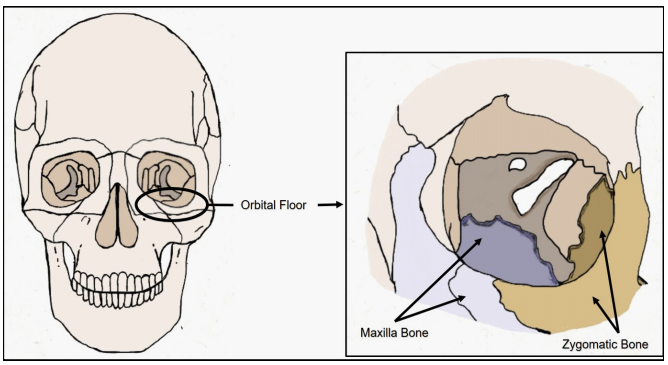

Figure 1: Orbital floor showing the maxilla and zygomatic bone.

Cite this article: Alhamoudi FH, Akhtar H, Almoshawah Y, Talari AC, Chaudhry AA, et al. Bioactive Nano Hydroxyapatites for Orbital Floor Repair and Regeneration. J Nanomed. 2021; 4(1): 1038.

Orbital floor bone is a natural composite material made up of organic and inorganic matrices, organic matrix being mostly collagen fibrils and the inorganic matrix comprising of mineral particles of hydroxy carbonated apatites. Synthetic Hydroxy-Apatite (HA) is similar to biological hydroxyapatite, the mineral component of bone, although it differs in crystallinity and chemical composition. Due to its osteoconductive nature and biocompatibility, HA has been used in bone repair and regeneration for a number of years. In addition, ionic substitution, such as carbonate, fluoride, phosphate, sodium, magnesium, silicon and citrate of HA can easily carried out, which improves both biocompatibility and bioactivity of these materials, playing an important role in bone repair and regeneration [4-8].

Recent studies have established that modification of functionalities on the surface of nanomaterials play an important role in bone repair and bone replacement. Therefore, alteration of the chemistry in synthetic HA has attracted significant attention in biomedical research, especially in scaffold development for tissue engineering applications, carriers for drugs, and control drug release [6].

The functional modification of HA in these applications is determined by the nanoscale morphology and crystallinity [9]. Moreover, the chemical and biological properties are known to depend on the crystal phases of HA. Therefore, techniques for the preparation of HA with a controlled structure would be highly useful for developing biologically suitable inorganic materials [10]. Over the past decades, many synthetic methods have been used to produce HA with various shapes and morphologies [11-17]. Due to its relatively economical production costs and simple synthetic processes, the hydrothermal technique (**Figure 2**) is an efficient synthesis method that produces materials with high crystallinity and nano morphological features that can be controlled [9,18].

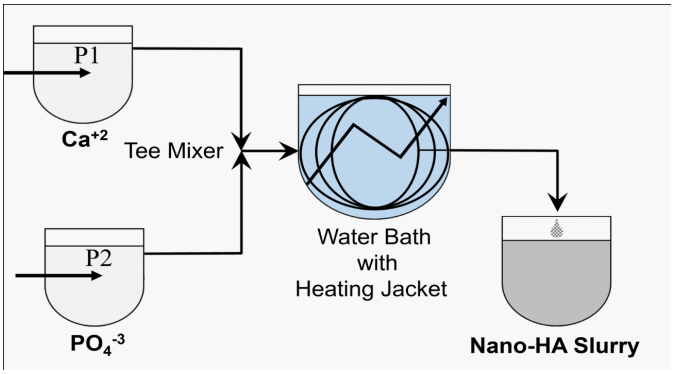

Figure 2: Hydrothermal process for HA synthesis. The technique uses two-pump (P1, P2) flow system for the synthesis of Stoichiometric and ionic substituted HA using a "T mixer". A water bath with heating jacket used for hydroxyapatite crystallisation [19].

The main minor substituent in bone apatite is carbonate ions, whose weight proportion can reach 2.0–8.0% in bone mineral [20]. If carbonate ions replace the OH^- ions in HA lattice (A-type substitution - minor) and the phosphate ions (B-type substitution - major) or replace two positions at the same time (AB-type substitution) [21,22]. The ratio of type A to type B in natural apatite is between 0.7 and 0.9, depending on the individual's age [8]. The B-type substitution in HA was influenced to cause an increase in solubility and a reduction in crystallinity in both *in vitro* and *in vivo* tests, resulted in better osteointegration and bioresorbability rate [23], while the human osteoblastic cells had a lower affinity for the Carbonate Hydroxyapatite (CHA) surface compared to HA [24,25]. Hence, carbonate substitution has minor effects on the structure and performance of HA.

Fluoride hydroxyapatite (fluorapatite, FHA), is synthesised by substituting OH^- with fluoride over a range of different concentrations. Recent studies have shown that fluoride substitution has enhanced mechanical properties and thermal stability [3,6]. FHA has good biocompatibility and low solubility compared to HA, which makes it a useful material for a number of dental applications [10]. Moreover, fluoride ions were demonstrated to increase HA's crystallization and mineralization during the bone development [26]. Furthermore, fluoride ions released from synthetic FHA can inhibit dental caries in a bacteria-containing acidic environment [7]. However, carbonate and fluoride substitution have conflicting outcomes on solubility and crystallinity in apatite. Therefore, managing the carbonate and fluoride combined substitution in the apatite allows to form a carbonate-fluoride-apatite as a bone graft material with tailored properties.

The nucleation and crystal growth of HA powders are affected by protein templates, such as collagen and some acidic molecules as they can be incorporated with calcium ions and produce calcium phosphate clusters in the early stage of mineralization [6,27]. 2% of bone's weight is an acidic molecule; citrate function remains a debatable factor in bone formation [28]. It has been suggested that citrate ions could induce the plate like morphology of amorphous precursor, increase the maturation time, and control the nanocrystals' thickness during the HA synthesis [29]. Furthermore, NMR studies have revealed strong interactions between HA and citrate molecules; the size of HA crystal is decreased as citrate concentration increases within the polymer matrix [30]. Davies *et al.* (2014) have summarised that the citrate anions could manage the assembling process of minerals in bone and link the HA platelets [28].

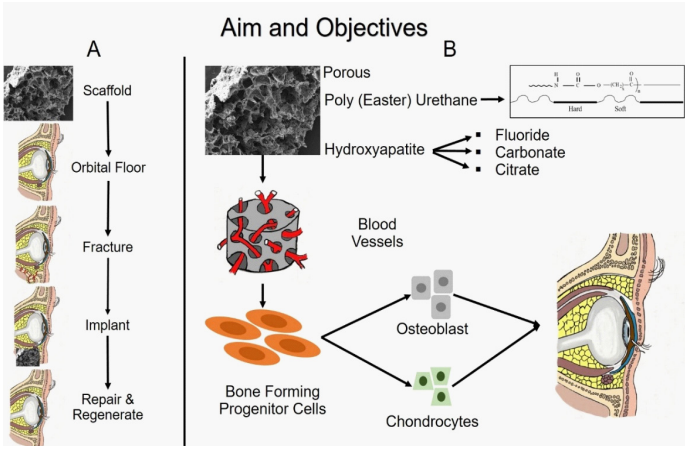

Figure 3: Graphical abstract **(A)**: the objective was to fabricate scaffolds for orbital floor repair and regeneration. **(B)**: Project materials and objectives. Synthesis of hydroxyapatites, carbonated-hydroxyapatites (CHA) and fluoro-hydroxyapatites (FHA), Grafting of these on Polyester-urethane via covalent bonding between the functional groups of apatites and the polyurethanes. These materials were used to fabricate bioactive scaffold with controlled porosity to achieve enhanced vascularisation.

Producing nanoceramic powders is crucially vital for bone tissue engineering applications to mimic natural bone architecture and teeth and produce better bioactivity [11,21,31,32]. The development of multi or co-substituted HA into the HA lattice is an exciting area of research trying to mimic the natural bone. Therefore, researchers have been concentrated on the multi substituted HA production, for instance, zinc citrate hydroxy-

apatites (zin-citHA), silicon carbonated hydroxyapatites (SiCHA) [31,33]. However, there have been no publication or any studies about the multi substitution of fluoride citrate HA, citrate carbonate HA or fluoride carbonate citrate HA. This study aims to synthesise multi substituted HA to be used with scaffolds for orbital floor fracture repair and regeneration. In this study, HA with carbonate substitution have been synthesised and their chemical, physical, and biological properties evaluated (**Figure 3**).

Materials and methods

Materials

Calcium Nitrate Tetra Hydrate ($Ca(NO_3)_2{\cdot}4H_2O$) (Acros Organics, USA) and Diammonium Hydrogen Phosphate ($(NH_4)2HPO_4$) (VWR Prolabo Chemicals, Belgium) were used as precursors, and Double-distilled water (H_2O) was used as a solvent. Liquid ammonia ((NH_4OH), 28-30%) (Honeywell Fluka, Germany) was used as a pH regulator. Ammonium Flouride (F), Sodium Hydrogen Carbonate (C), and Potassium Citrate (Cit) were used as carbonate and citrate source for HA substitution. P218R Hydroxyapatite was used as commercial HA (Plasma Biotal Limited, UK).

Methods

The molar ratio of Ca/P was fixed to 1.67. 0.5M of calcium nitrate tetrahydrate ($Ca(NO_3)_2{\cdot}4H_2O$) solution and a 0.3M diammonium hydrogen phosphate ($(NH_4)_2HPO_4$) solution were used as precursors.

The calcium nitrate tetrahydrate ($Ca(NO_3)_2{\cdot}4H_2O$) solution was prepared by dissolving calcium nitrate tetrahydrate in 100ml deionized water with continuous stirring at room temperature for an hour. Similarly, the diammonium hydrogen phosphate ($(NH_4)_2HPO_4$) solution was obtained by dissolving diammonium hydrogen phosphate into 100ml deionized water. The substituents fluoride (F), carbonate (C), and citrate (Cit) respectively were added as shown in **Table 1**. The molar ratio of Ca/P (1.67) is fixed in this method.

Table 1: The concentrations used for the substituting, where Ca=Calcium, P=Phosphate, F=Fluoride, C=Carbonate and Cit=Citrate.

	Ca + (Cit)	P + (F + C)
Stoichiometric HA	0.5	0.3
FHA	0.5	0.22 + (0.08)
CHA	0.5	0.22 + (0.08)
CitHA	0.42 + (0.08)	0.3
F-C-HA	0.5	0.22 + (0.04+0.04)
F-Cit-HA	0.46 + (0.04)	0.26 + (0.04)
C-Cit-HA	0.46 + (0.04)	0.26 + (0.04)
F-C-Cit-HA	0.473 + (0.0267)	0.247 + (0.0267+0.0267)

pH values of both solutions were measured by pH meter and the initial values were, pH 6.0 for calcium nitrate tetrahydrate and pH 8.0 for diammonium hydrogen phosphate. The optimum pH for the reaction was 10. To obtain this pH, ammonia solution (10ml) was added using dropwise via dropping funnel to each solution and pH was recorded at regular intervals till the optimum pH was reached.

The continuous hydrothermal synthesis method involved the aging of the reaction mixture at 90°C in a water bath. A silicon tube was inserted in each solution (diammonium hydrogen phosphate and calcium nitrate tetrahydrate) and these solutions were pumped through silicon tubes into the water bath with the help of a pump at flow rates of either 30 rpm 30ml/min or 60ml/min flow rates. Both solutions were run until they were consumed. The precursor solutions interacted at the T piece connecter used for mixing and followed by crystallization and the ageing process in a water bath 90°C for about 5 min. The reaction product was collected as white suspension via a silicon tube outlet into a glass flask.

The precipitates were filtered and washed with deionized water three times. The pH of the filtrate was recorded, and the washing process was repeated until pH 8 was achieved. The precipitate was collected in a glass petri dish and dried in an oven at 200°C for 24 hrs. The resulting powder was stored in a dry environment and its chemical, physical, mechanical and biological properties evaluated.

Fourier transform infrared spectroscopy (FTIR)

FTIR spectrometer iS50R™ (Thermo Nicolet, UK), in conjunction with a photoacoustic sampling (PAS) accessory (MTech™ PAS cell) was used in this study. PAS was used to characterize the bulk and neat samples, as it permitted analysis without any sample preparation. The sample chamber of the PAS cell was purged with helium gas to ensure a dry environment.

Spectral data acquisition and processing was carried out by using OMNIC™ version 9 software. Background spectrum was collected by using a carbon black film at 4 cm^1 resolution, accumulating 128 number of scans within the spectral range of 4000 to 400 cm^{-1}. HA powder was placed in a sample cup and analysed neat accumulating 128 number of scans within the spectral range of 4000 to 400 cm^{-1} at 4 cm^1 resolution.

Transmission electron microscopy (TEM)

Copper: palladium carbon-coated EM grids were glow discharged using an Agar Scientific Glow Discharge Unit attached to an Agar Scientific Turbo Carbon Coater Unit (Agar Scientific Stansted Essex UK). A 10µl drop of the sample was deposited onto the TEM grid for 30 seconds, after which any excess was removed by gently touching the edge of the grid with filter paper (Whatman grade 1 GE HealthCare UK, Little Chalfont, UK).

TEM grids were viewed in a FEI tecnai G2 Biotwin Transmission Electron Microscope (FEI Cambridge, UK) at an operating voltage of 80kv. Images were captured by a Gatan Orius 1000B digital camera using Gatan Digital Micrograph software suite (Gatan Ltd, Corby UK).

The synthesised HA particles' sizes were evaluated by ImageJ 1.50 software (Rasband, W.S., ImageJ, U. S. National Institutes of Health, Bethesda, Maryland, USA) on the TEM images.

Preparation of HA suspension for cell evaluation

The powder samples (Stoichiometric HA, FHA, CHA, CitHA, F-C-HA, F-Cit-HA, C-Cit-HA and F-C-Cit-HA) and the control group (commercial HA) were weighed (20 mg) in Eppendorf tubes, and were sterilised using Autoclave (for 30 minutes at 121°C) in water. Suspensions of sterilised powders were prepared by adding 1 mL of serum free media (DMEM media for MG63 and AMEM media for HTERT-BMSC; without) to each sample inside the cabinet and the autoclaved Eppendorf tubes with test pow-

der were sealed by parafilm strips to avoid contamination. The Ultra Sonic water bath was used for 1 hour to ensure that powders were well dispersed into suspension to form the stock solution (20mg/1ml), which was stored at -20°C.

The working solution were prepared from the suspension stock solution by two concentrations (0.1 and 0.2) mg/mL into media with serum (DMEM media for MG63 and AMEM media for HTERT-BMSC; without) to evaluate whether cell viability could be supported. The working solution were prepared freshly for each experiment and stored at 4°C during the experiment. The reason for the freshly prepared working solution was to avoid media oxidation.

Culture conditions for human osteoblast cell line (MG63)

The human osteosarcoma cell line MG63 was used for the assessment of cell viability. Cells were cultured and maintained at 37°C and 5% CO_2 with Dulbecco's Modified Eagle's Medium (DMEM) supplemented with 10% FBS (Advanced protein products, Brierley Hill, UK), 100 IU/mL penicillin, 100 µg/mL streptomycin, 2 mM glutamine, and 0.25% fungizone (Gibco Invitrogen, Paisley, UK).

Culture conditions for human telomerase reverse transcriptase-immortalized bone marrow mesenchymal stromal cells (hTERT-BMSCs)

The T75 flask was coated by adding 5ml of 0.1% gelatine solution (see protocol: Gelatine Solution). The flask was incubated for 30min at room temperature. The gelatine solution was discarded and the flask was ready for use. Cells were cultured and maintained at 37°C and 5% CO_2 with Alpha's modified eagle's medium (aMEM) supplemented with 10% FBS (Advanced protein products, Brierley Hill, UK), 100 IU/mL penicillin, 100 µg/mL streptomycin, 2 mM glutamine, and 0.25% fungizone (Gibco Invitrogen, Paisley, UK).

Assessment of cell attachment and cell viability

MG63 and HTERT-BMSC cells were seeded in 96-well flat-bottomed plates (Nunc, Nunclon™ Surface Roskilde, Denmark) at a concentration of 1 X 10^4 cells / well. The seeded cells were allowed to attach for 24 hrs. On culture day 1, culture medium was discarded and replaced with 100 µL of suspension containing the test powders. Samples were maintained at 37°C, 5% CO_2 in media (DMEM media for MG63 and AMEM media for HTERT-BMSC) for 24 hrs. For HTERT-BMSC cells, prior seeding the 96 well plates was coated by adding 1ml of 0.1% gelatine solution. The well plate was incubated for 30min at room temperature. The gelatine solution was discarded and the well plate was ready for use.

The metabolic activity of MG63 and HTERT-BMSC cells cultured with powders was measured by AlamarBlue® assay (AbD Serotec, Kiddlington, UK), absorbance (MG63) fluorescence (HTERT-BMSC) was measured at λ570 nm in a colorimetric plate reader (Bio-TEK, North Star scientific Ltd, Leeds, UK). Wells were then washed with PBS, media with 100 µL of the same suspensions added and the cells were returned to culture conditions. The AlamarBlue® assay was repeated on 3, 5 and 7 days of culture for MG63, and on 7, 14 and 21 days of culture for HTERT-BMSC. Cell-free samples in DMEM were included.

Statistical analysis

All experiments were conducted in triplicate and repeated three times (n=3 and N=3). Data are reported as mean ± standard deviation. Comparison of sample means of Alamar blue absorbance data was performed by one-way analysis of variance using GraphPad Prism. Differences between two groups were distinguished as statistically significant if $p \leq 0.05$ (*), $p \leq 0.01$ (**), $p \leq 0.001$ (***) and $p \leq 0.0001$ (****) as determined by the Turkey post-hoc test.

Results

Fourier transform infrared spectroscopy (FTIR)

The FTIR results confirmed that the synthesis of Stoichiometric HA, FHA, CHA, CitHA, F-C-HA, F-Cit-HA, C-Cit-HA and F-C-Cit-HA was successfully achieved (**Figures 4, and 5 and Table 2**).

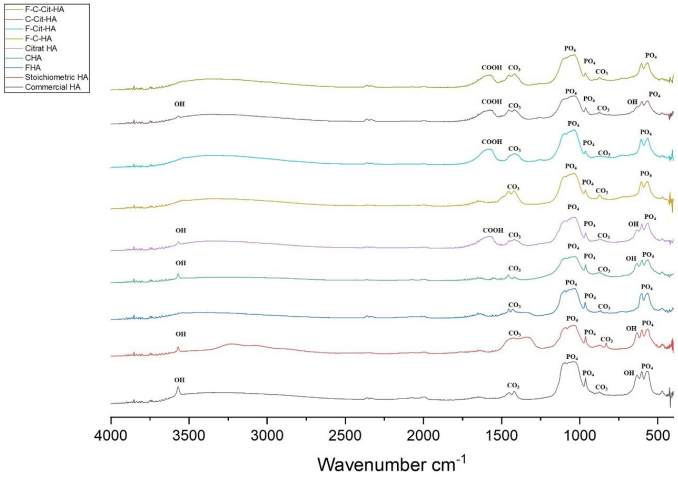

Figure 4: The FTIR spectra of commercial and synthesised HA including, stoichiometric and substituted apatites.

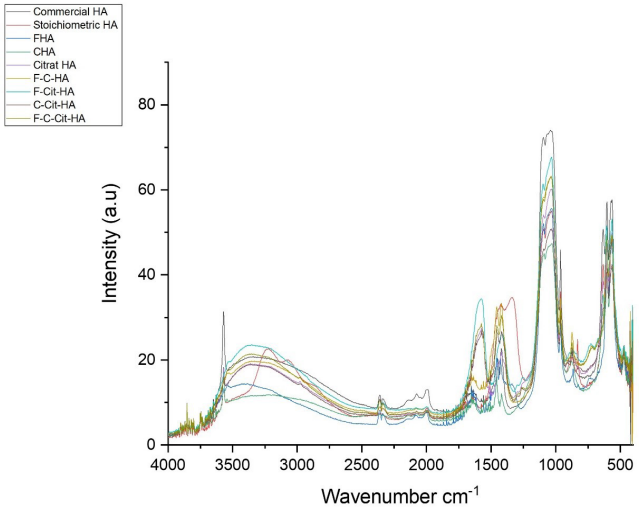

Figure 5: FTIR spectra of commercial and synthesised HA with different substitutions.

Table 2: The spectra peak positions of HA synthesis with different substitutions (HA=P218R commercially available HA from Plasma Biotal Limited, UK and Sto-HA=stoichiometric).

Functional Group	HA	Sto-HA	CitHA	CHA	FHA	C-Cit-HA	F-Cit-HA	F-C-HA	F-C-Cit-HA
OH	3570	3571	3569	3570	F	3568	F	F	F
	633	633	633	634	F		F	F	F
CO_3 A and B-Type	1453			1457	1454	1456		1456	1456
	1420	1334	1419	1419	1428	1419	1418	1421	1419
	876	875	875	879	865	875	867	874	874
PO_4	1039	1034	1030	1029	1031	1035	1032	1034	1035
	962	963	962	962	965	962	964	964	963
	604 & 564	602 & 566	602 & 564	602 & 563	605 & 565	602 & 565	607 & 565	607 & 567	605 & 565
COOH (citrates)			1576			1575	1575		1575.5

Transmission electron microscope (TEM)

The commercially available HA consisted of spherical particles (**Figure 6A**). Interestingly, the Stoichiometric HA prepared at 90°C had morphology of nano-roads (**Figure 6B**). The FHA, CHA, and F-C-HA also had nano-rods morphology, with more flake like structures (**Figure 6CDF**). However, HA with citrate (CitHA, F-Cit-HA, C-Cit-HA and F-C-Cit-HA) showed more needle like morphology (**Figure 6EGHI**). Most of HA particles were rod shaped, but citrate substitution produced more needle shaped particles.

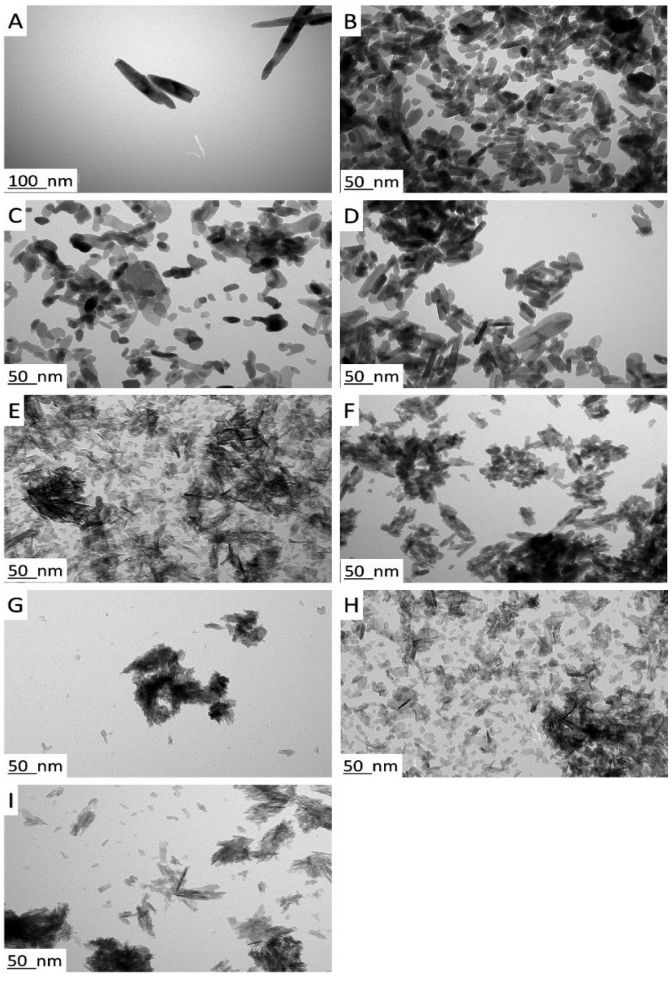

Figure 6: TEM images of substituted HA nanoparticles; **(A)** Commercial HA, **(B)** Stoichiometric HA , **(C)** FHA, **(D)** CHA, **(E)** CitHA, **(F)** F-C-HA, **(G)** F-Cit-HA, **(H)** C-Cit-HA and **(I)** F-C-Cit-HA.

The particle size of synthesised HA was significantly smaller than commercial HA (3806 nm^2), with a mean value of (1627nm^2). Moreover, CitHA has the smallest particles size 240 $nm^2 \pm 101.3$ compared to Pour HA (548 nm^2), FHA (828 nm^2) and CHA (1261 nm^2). Furthermore, the co-substitution HA (F-C-HA, F-Cit-HA, C-Cit-HA and F-C-Cit-HA) leads to a decrease in particles size compared to substituted HA (Stoichiometric HA, FHA, CHA and CitHA) significantly. The smallest particles size among all synthesised HA was in F-Cit-HA with particles size average 147 $nm^2 \pm 55.1$ (**Table 3, Figures 7 and 8)**.

Table 2: Particle size of hydroxyapatite as measured from TEM images using Image J.

HA	N total	Mean	Standard Deviation
Commercial HA	15	3806.48	1627.27
Stoichiometric HA	15	548.381	206.617
CHA	15	1261.82	517.343
FHA	15	828.65	239.304
CitHA	15	240.163	101.27
F-C-HA	15	444.931	154.317
F-Cit-HA	15	147.893	55.1264
C-Cit-HA	15	409.835	163.909
F-C-Cit-HA	15	207.428	87.0476

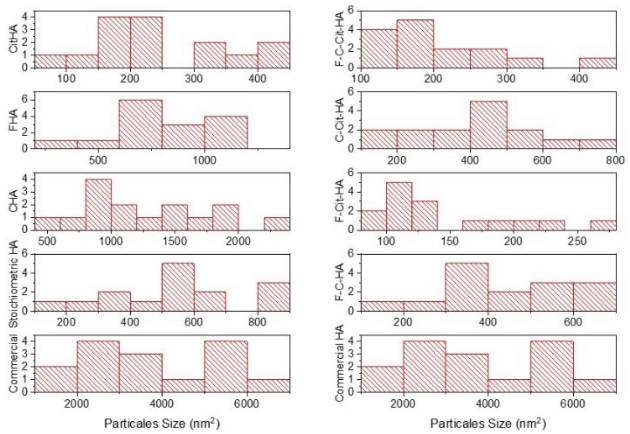

Figure 7: HA particle size distribution indicating that all synthesised hydroxyapatites were in the nano range. Citrate ion substitution led to a maximum reduction of the particle size.

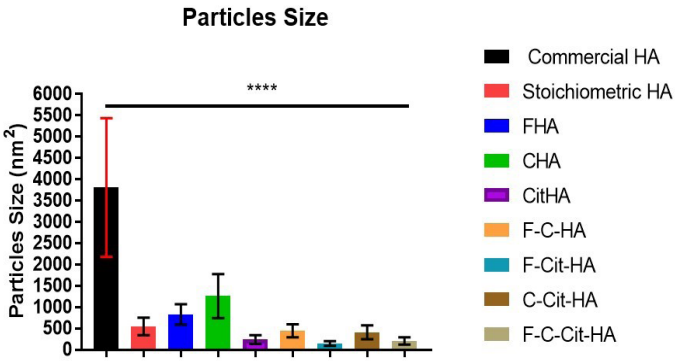

Figure 8: The particles size of synthesised HA (Stoichiometric HA, FHA, CHA, CitHA, F-C-HA, F-Cit-HA, C-Cit-HA and F-C-Cit HA) reduce compared to commercial HA significantly. Differences between two groups were distinguished as statistically significant if $p \leq 0.05$ (*), $p \leq 0.01$ (**), $p \leq 0.001$ (***) and $p \leq 0.0001$ (****) as determined by Turkey's post hoc pair-wise comparison.

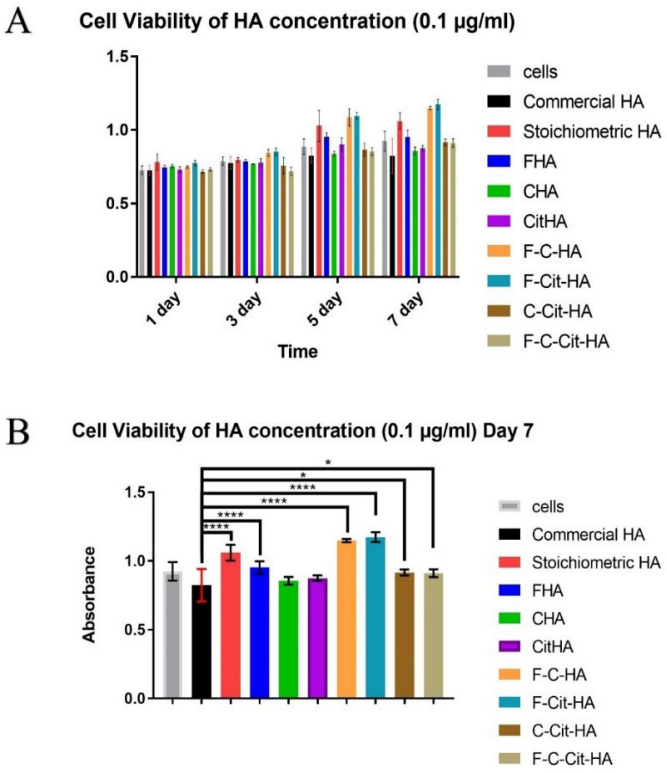

Figure 9: **(A)** cell viability over 7 days with MG63 for Commercial HA, Stoichiometric HA , FHA, CHA and CitHA, and co-substituted HA (F-C-HA, F-Cit-HA, C-Cit-HA and F-C-Cit-HA). Samples were used with concentration of 0.1 µg/ml in the suspension. **(B)** Significantly more cells were found on the 7th day with Stoichiometric HA , FHA, and co-substituted HA (F-C-HA and F-Cit-HA) compared with commercially available HA 'cells' indicates cells cultured in media with no sample added Differences between two groups were distinguished as statistically significant if $p \leq 0.05$ (*), $p \leq 0.01$ (**), p ≤ 0.001 (***) and p ≤ 0.0001 (****) as determined by the Turkey.

Assessment of cell attachment and cell viability

Human osteoblast cell line (MG63)

Human osteosarcoma cell line MG63 was used to evaluate the *in vitro* cell compatibility of synthesized hydroxyapatite and substituted hydroxyapatite over seven days. Cell viability assays indicated that none of the HA formation was toxic at a concentration of 0.1 µg/ml, (as seen by the increase in cell viability over time (**Figure 9A)**. However, some formations were shown to support higher cell viability, difference between formulations could be observed after 5 days of culture and statistical analysis at culture day 7 indicated there were significantly more metabolically active cells in cultures contain the suspensions of Stoichiometric HA , FHA, F-C-HA, F-Cit-HA, C-Cit-HA and F-C-Cit-HA than in commercial HA (**Figure 9B)**. For the 0.2 µg/ml concentration, there was some evidence of toxicity (as seen by lower cell viability at day 7 compared to day 1 **(Figure 10A)** in samples containing CHA and F-C-Cit-HA but other formations supported cell growth Stoichiometric HA , FHA, CHA, CitHA, F-C-HA, F-Cit-HA and C-Cit-HA by day 7 (**Figure 10B)**. The significant improvement was in samples with F-C-HA and F-Cit-HA. Commercial HA, Stoichiometric HA, FHA, CHA, CitHA, F-C-HA, F-Cit-HA, C-Cit-HA

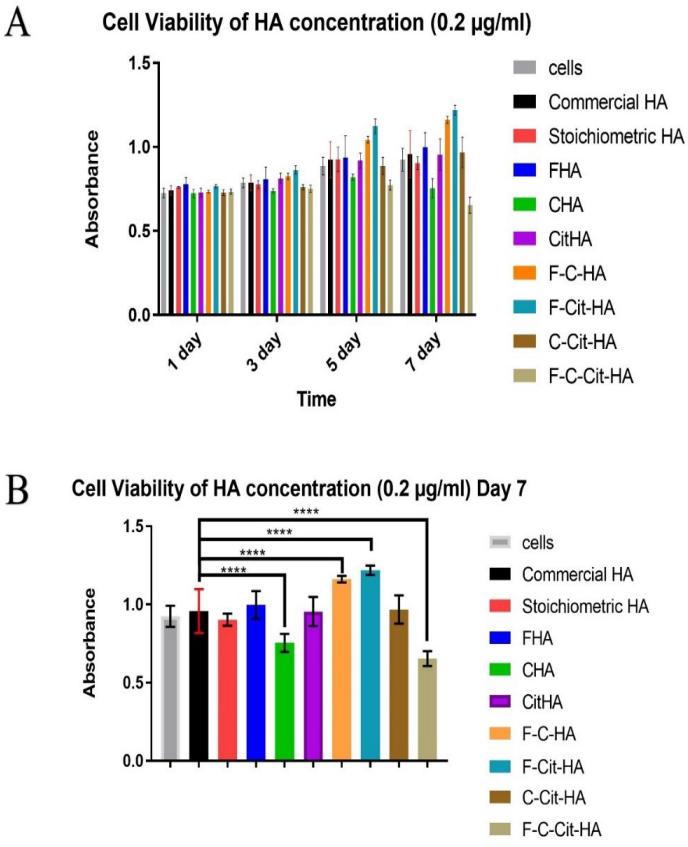

Figure 10: **(A)** Cell viability over 7 days with MG63 for Commercial HA, Stoichiometric HA , FHA, CHA and CitHA, and co-substituted HA (F-C-HA, F-Cit-HA, C-Cit-HA and F-C-Cit-HA). Samples were used with concentration of 0.2 µg/ml in the suspension. **(B)** Significant improvement on the 7th day with co-substituted HA (F-C-HA and F-Cit-HA) and significate decrease with CHA and F-C-Cit-HA. Differences between two groups were distinguished as statistically significant if $p \leq 0.05$ (*), $p \leq 0.01$ (**), $p \leq 0.001$ (***) and p ≤ 0.0001 (****) as determined by the Turkey.

Human telomerase reverse transcriptase-immortalized bone marrow mesenchymal stromal cells (hTERT-BMSCs)

The Primary Human Mesenchymal Stem Cells (hTERT-BMSCs) was used to evaluate the *in vitro* cell viability of synthesized hydroxyapatite and substituted hydroxyapatite over 21 days. Cell viability assays indicated that none of the HA formation was toxic at a concentration of 0.1 µg/ml and 0.2 µg/ml, (as seen by the increase in cell viability over time **(Figure 11A and Figure 12A)**. However, some formations were shown to support higher cell viability, difference between formulations could be observed after 7, 14 and 21 days of culture. The statistical analysis at culture day 21 indicated there were significantly more metabolically active cells in cultures containing the suspensions of stoichiometric HA, FHA, and citHA and F-Cit-HA than in commercial HA for the 0.1 µg/ml concentration **(Figure 11B)**. For the 0.2 µg/ml concentration, there were significantly more metabolically active cells in cultures contain the suspensions of CHA and F-Cit-HA HA than in commercial HA **(Figure 12B)**.

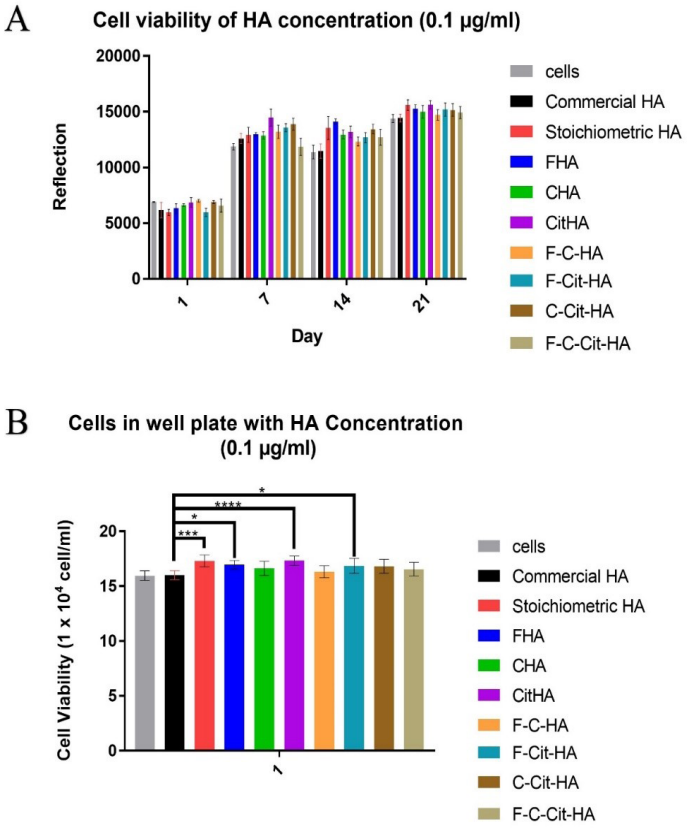

Figure 11: **(A)** Cell viability over 21 days with hTERT-BMSC for Commercial HA, Stoichiometric HA, FHA, CHA and CitHA, and co-substituted HA (F-C-HA, F-Cit-HA, C-Cit-HA and F-C-Cit-HA). Samples were used with concentration of 0.1 µg/ml in the suspension. **(B)** The significant improvement on 21 days cultured were with Stoichiometric HA, FHA, and citHA and F-Cit-HA. Differences between two groups were distinguished as statistically significant if $p \leq 0.05$ (*), $p \leq 0.01$ (**), $p \leq 0.001$ (***) and $p \leq 0.0001$ (****) as determined by the Turkey.

Discussion

FTIR spectra of the HA of various substituted formulations are given in **Figure 4 and Figure 5; Table 2**). Presence of hydroxyl group was evident from the spectral peak at 3568 – 3571 cm^{-1} in all HA samples except the HA substituted with F^-. The O–H peak intensity decreased with the substitution of carbonate and citrate. However, O–H peak disappeared with incorporation of

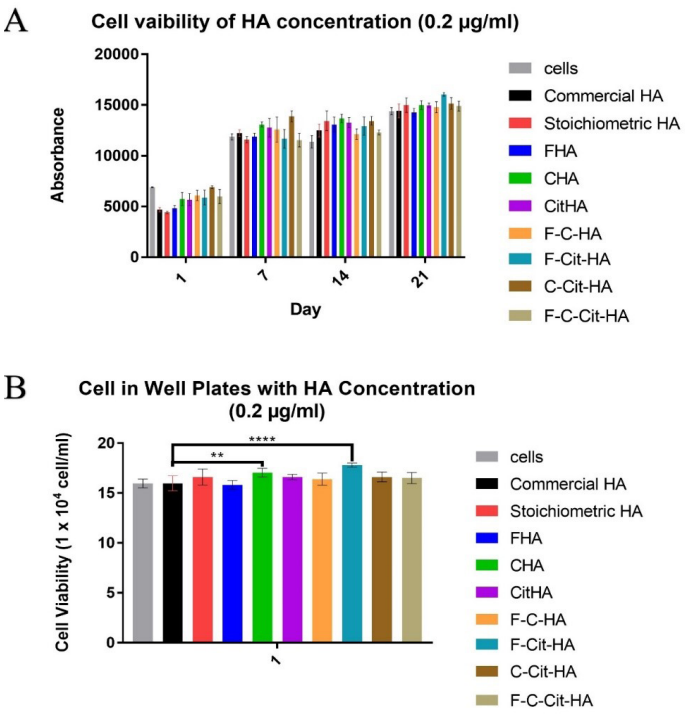

Figure 12: **(A)** cell viability over 21 days with hTERT-BMSC for Commercial HA, Stoichiometric HA, FHA, CHA and CitHA, and co-substituted HA (F-C-HA, F-Cit-HA, C-Cit-HA and F-C-Cit-HA). Samples were used with concentration of 0.2 µg/ml in the suspension. **(B)** The significant improvement on 21 days cultured were with CHA and F-Cit-HA HA. Differences between two groups were distinguished as statistically significant if $p \leq 0.05$ (*), $p \leq 0.01$ (**), $p \leq 0.001$ (***) and $p \leq 0.0001$ (****) as determined by the Turkey.

fluoride ions, indicating that the substitution or co-substitution of fluoride ion occupies the OH^- sites in the lattice structure [4,5,7]. The broad peak at 3220 - 3385 cm^{-1} is attributed to the presence of adsorbed water as well as the peak at 1653 cm^{-1} (**Figure 4 and Figure 5; Table 2**), which are shown in all HA except the HA with citrate [4,5,7].

The broad band at 1575 - 1576 cm^{-1} is due to C=O vibration from COOH group of citrate in all substituted HA samples (**Figure 4 and Figure 5, Table 2**). This confirmed the grafting of citrate in HA surface due to the shifting of C=O vibration from COOH group of citrate sodium from 1703 - 1752 cm^{-1} to 1575 - 1576 cm^{-1} in HA as reported by Verma et al. (2016) and Zhong et al. (2017) [6,29,37].

The spectral peaks present at 1453 - 1457 cm^{-1} are attributed to A-type carbonate, whereas the peaks at 1334 - 1428 cm^{-1} are assigned to B-type carbonate, and 865 – 879 cm^{-1} appeared in all HA, except for the HA with citrate where the peak at 1453 - 1457 cm^{-1} disappeared **(Figure 4, Figure 5 &Table 2)**. This indicated that the HA grafted with citrate had B-type site carbonate, but when the citrate HA substituted with carbonate, peak appeared at 1453 - 1457 cm^{-1} in high intensity changing the carbonate to be in A-type site. Similarly, HA substituted with Fluoride or carbonate had A-type site carbonate, due to which the 1453 - 1457 cm^{-1} band appeared in higher intensity than that of 1334 - 1428 cm^{-1}[18]. These results are in agreement with the findings reported by Rehman and Bonfield (1997) Kovaleva et al. (2008) and Zhu et al. (2015), where the A-type site carbonate existed above 0 – 4 wt. % range of carbonate [4,8,37,38].

However, HA, which co-substituted with fluoride and carbonate, have less peak intensity at 1453 - 1457 cm^{-1} than 1334 - 1428 cm^{-1} [4], indicating that the substitution priority of fluoride for OH^- has changed the carbonate substitution type and compelled most of the carbonate to be located in the B sites **(Figure 4 and Figure 5, Table 2)**. This was similar to the results of HA that grafted with citrate and co-substituted with fluoride and carbonate. Moreover, this was the case with commercial and Stoichiometric HA.

The other spectral peaks of phosphate modes are assigned as, 1029 - 1039 cm^{-1} (phosphate asymmetric stretching vibration), 962 - 965 cm^{-1} (phosphate symmetric stretching vibration), 602 – 607 cm^{-1} and 563 - 567 cm^{-1} (phosphate bending vibration) and were observed in all samples representing the typical bands of apatite [4,7] **(Figure 4 and Figure 5, Table 2)**. FTIR results indicating successful synthesis of Stoichiometric HA , substituted HA (FHA, CHA and CitHA) and co-substituted HA (F-C-HA, C-Cit-HA, F-Cit-HA and F-C-Cit-HA) with hydrothermal methods.

The results of TEM have shown that the synthesised HA were in rod shaped, but the HA with citrate substitution produced more needle shaped particles (**Figure 6**). Furthermore, the particle size of synthesised HA were reduced with the substitution compared to commercial HA **(Table 3 & Figure 7, Figure 8)** [4,7,29,39,40]. The substituted or co-substituted HA with citrate have smaller particle size compared to the rest of synthesised HA **(Table 3 & Figure 7, Figure 8)**, due to the effect of citrate on HA crystal size. This is in agreement with the results already reported in literature [30,33,37,41]. In this study, particle size and shape was controlled by carrying out type and amount of substitutions within the HA lattice structure, which plays a pivotal role is bone repair and regeneration, as it helps in controlling the bioactivity and biocompatibility of these nanoceramics [11,21,31,32].

To investigate whether the substituted HA formulations were able to support cell viability of osteoblasts and mesenchymal stem cells metabolic activity of the cells cultured in two concentrations of the powders was measured over time. As shown in (**Figure 11B & Figure 12B**), there was an increase in hTERT-BMSCs cell viability over 21 days on all HA, however, in contrast to MG63 cells over 7 days (**Figure 9B & Figure 10B**); there was no decrease in their ability to support cell proliferation compared to commercial HA. MG63 cell viability decreased significantly with CHA and F-C-Cit-HA by increasing the concentration from 0.1 µg/ml to 0.2 µg/ml compared to commercial HA. This was different in hTERT-BMSCs cell viability with F-C-Cit-HA as no decrease happened, where the CHA showed a significant improvement by increasing the concentration to 0.2 µg/ml compared to commercial HA. MG63 and hMCS showed similar results as the cells viability were improved significantly with Stoichiometric HA, FHA and F-Cit-HA in 0.1 µg/ml concentration, and by increasing the concentration to 0.2 µg/ml F-Cit-HA showed a significant improvement compared to commercial HA. There is no apparent cause for this differential effect of nHA on cell proliferation of the two types it could be associated with their different stages in the osteogenic differentiation pathways [42], may be related to the different time periods. However, there is an overall improvement of cell viability for F-Cit-HA. The reason could be the size of the nanoparticles of synthesized HA which increases the surface area leading to improved cell adhesion as already reported in litertaure [42].

The chemical composition of inorganic matrix of natural bone has a similarity to hydroxyapatite ($Ca_{10}(PO_4)_6(OH)_2$,HA) [8]. However, as the HA is the most stable material and least soluble among the calcium phosphates may impede the rate of bone regeneration upon implantation [25]. Based on the *in vitro* results, the interaction between cell and HA gets affected by the concentration of substitutions in HA lattice [31,43,44].

Carbonate apatite exhibits a chemical composition closer to bone or dental enamel than that of HA [45]. The presence of carbonate in synthetic HA leads to faster bonding between an inserted implant surface and human bone [21,46] due to the improvement in HA solubility by the presence of carbonate in HA lattice, which resulted in enhanced biological activity of HA [47]. A comparison of micro and nano CHA have already been reported in literature, both the CHA ceramics showed higher bioactivity than the micro HA over 7 days cell culture, whereas it was significantly higher for nanoceramic [46]. Results in our study are in agreement with these findings, as CHA showed improvement over 21 days with hTERT-BMSC, but with MG63 the results showed decrease in cell viability. In another study, the substitution or co-substitution of HA with silicon (Si) and carbonate were evaluated in hTERT-BMSC. It showed that HA containing higher amount of carbonate showed higher proportion of viable cells, particularly CHA and the C/Si HA (with less Si 0.8 (wt. %) compared to 5.2 (wt. % carbonate)) [31]. This is in agreement with the results obtained in this study as 0.2 µg/ml concertation of CHA on hTERT-BMSC showed significant improvement of cell viability (**Figure 12B**). Whereas, with 0.1 µg/ml concentration, the co-substituted HA (such as F-C-HA, C-Cit-HA or F-C-Cit-HA), where carbonate amount reduced, showed less cell viability (**Figure 11B**). Furthermore, increasing carbonate amount in HA lead to reduced cell viability significantly with 0.2 µg/ml concentration in the case of MG63 (**Figure 10B**).

In the literature, higher cellular responses for the FHA have been reported, which could be due to the effect of fluoride ion, as it is well known effect that it improves bone formation *in vivo*, and promotes remineralization and calcification [26,48,49]. Chemically, the OH^- groups in the HA supply binding sites for cell absorption, when the OH^- groups are replaced by fluoride in the FHA leading to an increase of the material surface negative charges (**Figure 4** & **Figure 5**). This may improve the cell attachment and subsequent cell activities along with increasing fluoride and culturing time which has also been reported in a number of studies [42,50,51]. However, the cell response improves when the fluorine ion concentration administrated within appropriate range in HA lattice. Less than 40% of fluoride in HA lattice could improve cell viability, where more than 40% may lead to cell stress and death [43,44]. This was confirmed in this study as well, either substituted or co-substituted HA with fluoride showed a significant improvement in cell viability on MG63s and hTERT-BMSC.

In 1960, it was discovered that citrate molecules are relatively rich in the organic bone components (5% wt) [52]. The majority of body citrate around (80 wt%) is stored in bone [41]. Citrate plays a role in the biomineralization process by controlling the interaction between citrate and collagen [53], and stabilizing nanoparticles of HA in bone tissue [54]. Recently, it was reported that the tightly bound citrate molecules are studded on the apatite surface [28,54]. The target of repairing and regenerating fractured bone is to mimic the structural, functional and biomechanical properties of the native bone. For this target to be achieved, the new regenerative bone structural must in-

clude the appropriate incorporation of citrate. However, there is a limitation about the citrate content and its incorporation in osteoinductive bone products [55]. The results of TEM showed that the presence of citrate in HA lattice led to control size in the particles as well as in co-substituted (F-Cit-HA, C-Cit-HA, F-C-Cit-HA) (**Figure 6** & **Figure 7 & Figure 8 & Table 3**). This has been reported in a number of studies [30,33,37,41]. Moreover, it has been explained that the released citrate can increase the hTERT-BMSCs differentiation by controlling energy-producing metabolic pathways, via active bone-forming cells [56,57]. The presence of citrate either in substituted (CitHA) or co-substituted HA (F-Cit-HA, C-Cit-HA, F-C-Cit-HA) promote cell viability not only with hTERT-BMSCs but also with MG63, particularly in the case of F-Cit-HA. In another recent study, it has been reported that substituted and co-substituted HA with zinc and/or citrate presented an improvement of the cell growth, particularly with zinc-cit-HA. However, the CitHA was similar to other samples after day 12 and 18 cultured days [33]. This indicated that citrate is able to influence the biological outcome, epically when co-substituted.

Findings of this study supports the possible use of the carbonate, fluoride, and/or citrate substituted apatite, specifically the F-Cit-HA, in the scaffolds fabrication, coating materials and an injectable gel for bone repair and regeneration, specifically for orbital floor repair an regeneration.

Conclusion

The synthesis of Hydroxyapatites with substitution (fluoride, carbonate and citrate) leads to reduction in particles size compared to commercial and stoichiometric hydroxyapatites. Furthermore, the co-substituted hydroxyapatite resulted in nanosized needle-like morphology compared to substituted hydroxyapatites, specifically for citrate substituted samples. Efficient cell attachment and viability can be achieved by controlled ionic substitution within the lattice structure of HA. However, the presence of citrate either in substituted (CitHA) or co-substituted HA (F-Cit-HA, C-Cit-HA, F-C-Cit-HA) promote cell viability not only with hTERT-BMSCs but also with MG63. These results confirm that incorporation of Fluoride and Citrate ions in HA lattice structure is the future direction of research for bone repair and regeneration, as their incorporation enhances bioactivity and cell viability.

Acknowledgments

The authors are grateful to the Ministry of Education of Saudi Arabia for the funding of this PhD studentship.

References

1. Dubois L, Steenen SA, Gooris PJJ, Mourits MP, Becking AG. Controversies in orbital reconstruction - II. Timing of post-traumatic orbital reconstruction: A systematic review. Int J Oral Maxillofac Surg. 2015; 44: 433-440.

2. Kanno T, Tatsumi H, Karino M, et al. Applicability of an Unsintered Hydroxyapatite Particles/Poly-L-Lactide Composite Sheet with Tack Fixation for Orbital Fracture Reconstruction. J Hard Tissue Biol. 2016; 25: 329-334.

3. Bartoli D, Fadda MT, Battisti A, et al. Retrospective analysis of 301 patients with orbital floor fracture. J Cranio-Maxillofacial Surg. 2015; 43: 244-247.

4. Zhu QX, Li YM, Han D. Co-substitution of carbonate and fluoride in hydroxyapatite: Effect on substitution type and content. Front Mater Sci. 2015; 9: 192-198.

5. Barry AB, Zhuang H, Baig AA, Higuchi WI. Effect of fluoride pretreatment on the solubility of synthetic carbonated apatite. Calcif Tissue Int. 2003; 72: 236-242.

6. Verma G, Barick KC, Shetake NG, Pandey BN, Hassan PA. Citrate-functionalized hydroxyapatite nanoparticles for pH-responsive drug delivery. RSC Adv. 2016; 6: 77968-77976.

7. Khan AS, Aamer S, Chaudhry AA, Wong FSL, Rehman IU. Synthesis and characterizations of a fluoride-releasing dental restorative material. Mater Sci Eng C. 2013; 33: 3458-3464.

8. Rehman I, Bonfield W. Characterization of hydroxyapatite and carbonated apatite by photo acoustic FTIR spectroscopy. J Mater Sci Mater Med. 1997; 8: 1-4.

9. Chaudhry AA, Yan H, Gong K, Inam F, Viola G, et al. High-strength nanograined and translucent hydroxyapatite monoliths via continuous hydrothermal synthesis and optimized spark plasma sintering. Acta Biomaterialia. 2011; 7: 791-799.

10. Chen M, Jiang D, Li D, Zhu J, Li G, et al. Controllable synthesis of fluorapatite nanocrystals with various morphologies: Effects of pH value and chelating reagent. J Alloys Compd. 2009; 485: 396-401.

11. Chaudhry AA, Haque S, Kellici S, et al. Instant nano-hydroxyapatite: A continuous and rapid hydrothermal synthesis. Chem Commun. 2006: 2286.

12. Fujishiro Y, Yabuki H, Kawamura K, Sato T, Okuwaki A. Preparation of needle-like hydroxyapatite by homogeneous precipitation under hydrothermal conditions. J Chem Technol Biotechnol. 1993; 57: 349-353.

13. Liu DM, Troczynski T, Tseng WJ. Water-based sol-gel synthesis of hydroxyapatite: Process development. Biomaterials. 2001; 22: 1721-1730.

14. Shum HC, Bandyopadhyay A, Bose S, Weitz DA. Double emulsion droplets as microreactors for synthesis of mesoporous hydroxyapatite. Chem Mater. 2009; 21: 5548-5555.

15. Seo DS, Lee JK. Synthesis of hydroxyapatite whiskers through dissolution-reprecipitation process using EDTA. J Cryst Growth. 2008; 310: 2162-2167.

16. Liu J, Li K, Wang H, Zhu M, Xu H, et al. Self-assembly of hydroxyapatite nanostructures by microwave irradiation. Nanotechnology. 2005; 16: 82-87.

17. Chen H, Sun K, Tang Z, et al. Synthesis of fluorapatite nanorods and nanowires by direct precipitation from solution. Cryst Growth Des. 2006; 6: 1504-1508.

18. Anwar A, Rehman IU, Darr JA. Low-Temperature Synthesis and Surface Modification of High Surface Area Calcium Hydroxyapatite Nanorods Incorporating Organofunctionalized Surfaces. J Phys Chem C. 2016; 120: 29069-29076.

19. Anwar A, Rehman IU, Darr JA. Low-Temperature Synthesis and Surface Modification of High Surface Area Calcium Hydroxyapatite Nanorods Incorporating Organofunctionalized Surfaces. J Phys Chem C. 2016; 120: 29069-29076.

20. Kay MI, Young RA, Posner AS. Crystal structure of hydroxyapatite. Nature. 1964; 204: 1050.

21. Chaudhry AA, Knowles JC, Rehman I, Darr JA. Rapid hydrothermal flow synthesis and characterisation of carbonate and silicate-substituted calcium phosphates. J Biomater Appl. 2013; 28: 448-461.

22. Ślósarczyk A, Paszkiewicz Z, Paluszkiewicz C. FTIR and XRD evaluation of carbonated hydroxyapatite powders synthesized by wet methods. J Mol Struct. 2005; 744-747(SPEC. ISS.): 657-661.

23. Morales-Nieto V, Navarro CH, Moreno KJ, et al. Poly (methyl methacrylate)/carbonated hydroxyapatite composite applied as coating on ultra high molecular weight polyethylene. Prog Org Coatings. 2013; 76: 204-208.

24. Landi E, Tampieri A, Celotti G, Vichi L, Sandri M. Influence of synthesis and sintering parameters on the characteristics of carbonate apatite. Biomaterials. 2004; 25: 1763-1770.

25. Landi E, Celotti G, Logroscino G, Tampieri A. Carbonated hydroxyapatite as bone substitute. J Eur Ceram Soc. 2003; 23: 2931-2937.

26. Grzanna M, LeGeros RZ, Polotsky A, Lin SJ, Hungerford DS, Frondoza C. Fluoride-substituted apatites support proliferation and expression of human osteoblast phenotype in vitro. In: Key Engineering Materials. Trans Tech Publ. 2003; 240: 695-698.

27. Cölfen H. Biomineralization: A crystal-clear view. Nat Mater. 2010; 9: 960.

28. Davies E, Müller KH, Wong WC, et al. Citrate bridges between mineral platelets in bone. Proc Natl Acad Sci. 2014; 111: E1354-E1363.

29. Zhong Z, Qin J, Ma J. Rapid synthesis of citrate-zinc substituted hydroxyapatite using the ultrasonication-microwave method. Ceram Int. 2017; 43: 13308-13313.

30. Hu Y-Y, Liu XP, Ma X, et al. Biomimetic self-assembling copolymer– hydroxyapatite nanocomposites with the nanocrystal size controlled by citrate. Chem Mater. 2011; 23: 2481-2490.

31. Ismail YMB, Wimpenny I, Bretcanu O. In Vitro Biocompatibility of SiCHA Nanopowders on Human Mesenchymal Stem Cells. 2018; 14: 35-46.

32. Dorozhkin SV. Nanodimensional and Nanocrystalline Calcium Orthophosphates. 2012; 2: 48-97.

33. Fernandes MH, Alves MM, Cebotarenco M, Ribeiro IAC. Materials Science & Engineering C Citrate zinc hydroxyapatite nanorods with enhanced cytocompatibility and osteogenesis for bone regeneration. Mater Sci Eng C. 2020; 115: 111147.

34. Manoj M, Subbiah R, Mangalaraj D, Ponpandian N, Viswanathan C, Park K. Influence of Growth Parameters on the Formation of Hydroxyapatite (HAp) Nanostructures and Their Cell Viability Studies. Nanobiomedicine. 2015; 2: 2.

35. Kaur G, Pickrell G, Kimsawatde G, Homa D, Allbee HA, et al. Synthesis, cytotoxicity, and hydroxyapatite formation in 27-Tris-SBF for sol-gel based CaO-P2O5-SiO2-B2O 3-ZnO bioactive glasses. Sci Rep. 2014; 4: 1-14.

36. Szymonowicz M, Korczynski M, Dobrzynski M, et al. Cytotoxicity evaluation of high-temperature annealed nanohydroxyapatite in contact with fibroblast cells. Materials (Basel). 2017; 10.

37. Zarif F, Tabassum S, Jamal A, et al. Surface - grafted remedial hydroxyapatite nanoparticles to avoid operational infections. Monatshefte für Chemie - Chem Mon. 2019; 150: 605-615.

38. Kovaleva ES, Shabanov MP, Putlayev VI, Filippov Y, Tretyakov YD, et al. Carbonated hydroxyapatite nanopowders for preparation of bioresorbable materials. Materwiss Werksttech. 2008; 39: 822-829.

39. Sun R, Yang L, Zhang Y, et al. Novel synthesis of AB-type carbonated hydroxyapatite hierarchical microstructures with sustained drug delivery properties. CrystEngComm. 2016; 18: 8030-8037.

40. Othman R, Mustafa Z, Loon CW, Noor AFM. Effect of Calcium Precursors and pH on the Precipitation of Carbonated Hydroxyapatite. Procedia Chem. 2016; 19: 539-545.

41. Santos C, Almeida MM, Costa ME. Morphological Evolution of Hydroxyapatite Particles in the Presence of Di ff erent Citrate: Calcium Ratios. 2015.

42. Nathanael AJ, Mangalaraj D, Hong SI, Masuda Y, Rhee YH, et al. In fluence of fl uorine substitution on the morphology and structure of hydroxyapatite nanocrystals prepared by hydrothermal method. Mater Chem Phys. 2013; 137: 967-976.

43. Nasker P, Samanta A, Rudra S, Sinha A, Mukhopadhyay AK, et al. Journal of the Mechanical Behavior of Biomedical Materials E ff ect of fl uorine substitution on sintering behaviour, mechanical and bioactivity of hydroxyapatite. J Mech Behav Biomed Mater. 2019; 95: 136-142.

44. Nasker P, Mukherjee M, Kant S, Tripathy S, Sinha A. Fluorine substituted nano hydroxyapatite : Synthesis, bio-activity and antibacterial response study. Ceram Int. 2018; 44: 22008-22013.

45. Elliott JC, Holcomb DW, Young RA. Infrared determination of the degree of substitution of hydroxyl by carbonate ions in human dental enamel. Calcif Tissue Int. 1985; 37: 372-375.

46. Li B, Liao X, Zheng L, et al. Preparation and cellular response of porous A-type carbonated hydroxyapatite nanoceramics. 2012; 32: 929-936.

47. Bonfield W, Gibson IR. Novel synthesis and characterization of an AB-type carbonate-substituted hydroxyapatite. J Biomed Mater Res. 2002; 59: 697-708.

48. LeGeros RZ. Calcium phosphates in oral biology and medicine. Monogr oral Sci. 1991; 15: 109-111.

49. LeGeros RZ, Silverstone LM, Daculsi G, Kerebel LM. In vitro caries-like lesion formation in F-containing tooth enamel. J Dent Res. 1983; 62: 138-144.

50. Eslami H, Solati-hashjin M, Tahriri M. The comparison of powder characteristics and physicochemical , mechanical and biological properties between nanostructure ceramics of hydroxyapatite and fl uoridated hydroxyapatite. Mater Sci Eng C. 2009; 29: 1387-1398.

51. Jazayeri HE, Tahriri M, Razavi M, et al. A current overview of materials and strategies for potential use in maxillofacial tissue regeneration. Mater Sci Eng C. 2017; 70: 913-929.

52. Taylor TG. The nature of bone citrate. Biochim Biophys Acta. 1960; 39: 148-149.

53. Shao C, Zhao R, Jiang S, et al. Citrate improves collagen mineralization via interface wetting: A physicochemical understanding of biomineralization control. Adv Mater. 2018; 30: 1704876.

54. Hu Y, Rawal A. Strongly bound citrate stabilizes the apatite nanocrystals in bone. 2010; 2010.

55. Costello LC, Chellaiah M, Zou J, Franklin RB, Mark A. HHS Public Access. 2015.

56. Fu X, Li Y, Huang T, et al. Runx2 / Osterix and Zinc Uptake Synergize to Orchestrate Osteogenic Differentiation and Citrate Containing Bone Apatite Formation. 2018; 1700755.

57. He Y, Li Q, Ma C, et al. Acta Biomaterialia Development of osteopromotive poly (octamethylene citrate glycerophosphate) for enhanced bone regeneration q. 2019; 93: 180-191.